Linear robust output–feedback control for permanent–magnet synchronous motors with unknown load

Antonio Loria

Robust Linear Control of (Chaotic) Permanent-Magnet Synchronous Motors With Uncertainties

Antonio Loría, *Member, IEEE*

***Abstract*—We solve the problem of set-point (respectively, tracking) control of a permanent-magnet synchronous motor via *linear* time-invariant (respectively, time varying) control. Our control approach is based on the physical properties of the machine: inherent stability and robustness to external disturbances. Our analysis is carried out under mild conditions, using *cascaded* systems theory. For all cases: constant operating point, trajectory tracking, and with known and unknown load, we show uniform global asymptotic stability of the closed-loop system with a linear controller that uses only velocity measurements. Furthermore, we explore natural extensions of our results to improve robustness with respect to external "disturbances" and parametric uncertainties.**

***Index Terms*—Chaos, output feedback control, PMSM, synchronization, synchronous motor.**

I. Introduction

THE analysis and control of chaos in electrical machines operations is of increasing interest cf., [1], [2]. In this paper, we revisit the problems of set-point (constant operating point) and tracking (time-varying operating regime) control of open-loop chaotic permanent-magnet synchronous machines (PMSM). This problem has attracted a number of researchers from different areas as witnessed by the variety of publications' fora: physics cf., [3], [4], (power) electronics cf., [5]–[7], electrical engineering (circuits) cf.,[8]–[12]; besides the fact that the PMSM is a popular benchmark in the control community cf., [13], [14]. One of the key problems related to the PMSM is its natural *chaotic* behavior, for certain choices of parameters and initial conditions, see, e.g., [15], [16], [6], [11].

In some of the cited works the control goal is to stabilize the system to a constant operating point. Typically, this means a constant shaft angular velocity. As is often desirable in control theory and practice, the control goal is to be achieved for all initial conditions, i.e., one seeks for *global* results. Of particular interest (at least in electrical engineering and physics) is to drive the PMSM to a constant operating point from initial conditions leading to chaos in open loop cf., [8], [10], [14]. The latter two exploit the Hamiltonian structure of the PMSM, the design in [14] leads to a closed-loop system with multiple equilibria, and the result is shown to hold for *almost* all initial conditions. While no stability proof is provided in [8], the control is interesting in that it exploits the dissipative forces inherent in the system and yields good performance, in *simulations*. Adaptive set-point control algorithms are included in [14] (known parameters, unknown load) and in [4] (zero load, one unknown parameter, smooth-air-gap machine). Other papers aiming at annihilating chaos include [15] where the goal is to drive the machine to describe periodic orbits.

Following an opposite train of thought, other works concentrate into *generating* chaos in the PMSM. Indeed, while it has been argued that chaos is undesirable for a number of relatively valid reasons, it is also argued the opposite with certain interesting applications in mind: [3] presents a controller to generate chaotic behavior in PMSMs used to construct vibratory soil compactors. Simulation results are presented in [5], where chaos is induced via delayed feedback.

With a grasp on the physical properties of the PMSM, in this paper, we take a control and stability viewpoint on the problems of set point (eliminate chaos) and tracking control (produce chaos) for the PM synchronous machine. We propose very simple output feedback control laws and show that uniform exponential stability may be achieved; in the case that the torque load is unknown, we use adaptive control. The term "output feedback" corresponds to shaft angular velocity measurements. We also show (analytically) that the output feedback controllers are robust with respect to additive disturbances, and (in simulations) with respect to measurement noise and parametric time-varying uncertainties. As a direct corollary of the main results several natural modifications, along the lines of similar results from the literature (without proof or with known load or only for set-point control—cf., e.g., [8]), may be introduced to improve robustness. Simulation results are presented to illustrate our theoretical findings.

The rest of the paper is organized as follows. In Section II, we present the dynamic model; in Section III, we describe the cascades-based control approach that we follow to solve the set-point control problem—cf., Section IV— and tracking control problem—cf. Section V. In Section VI, we discuss robustness properties. In Section VII, we present several simulation results and we conclude with some remarks in Section VIII. Some material on stability theory is presented in the Appendix.

Manuscript received May 19, 2008; revised October 01, 2008. First published December 22, 2008; current version published September 11, 2009. This paper was recommended by Associate Editor C. K. Tse.

The author is with French National Centre of Scientific Research (CNRS), Laboratoire de Signaux et Systemes, Supelec (LSS-SUPELEC), 91192 Gif-sur-Yvette, France (e-mail: loria@lss.supelec.fr).

Digital Object Identifier 10.1109/TCSI.2008.2011587

II. Model

A. "Physical" Model

The dynamic model of the PM synchronous machine on the $d-q$ axis is given by—cf., e.g., [15], [17], [8]

$$\frac{di_d}{dt'} = \frac{1}{L_d}[v_d - Ri_d + \omega L_q i_q] \tag{1a}$$

$$\frac{di_q}{dt'} = \frac{1}{L_q}[v_q - Ri_q - \omega L_d i_d - \omega\psi_r] \tag{1b}$$

$$\frac{d\omega}{dt'} = \frac{1}{J}[n_p\psi_r i_q + n_p(L_d - L_q)i_d i_q - \tau_L - \beta\omega] \tag{1c}$$

where t' denotes time. The variables carrying the index q are referred to the quadrature-axis and those carrying an index d are referred to the direct-axis. As is customary the variables i represent currents, v represent input voltages (control inputs up to a gain); L_q, L_d are stator inductances and R corresponds to the stator resistance. The rest of the variables represent the permanent-magnet flux (ψ_r), the number of pole pairs n_p, the viscous friction coefficient (β), and the polar moment of inertia (J). The angular velocity is represented by ω and, finally, τ_L corresponds to the external-load torque. The latter two are of obvious practical interest from a control viewpoint.

Model (1) is expressed in d–q coordinates, i.e., after performing a coordinate transformation that renders rotor inductances constant—cf., [17], [11] as opposed to rotor-position dependent. The starting point goes farther to a unified theory of electrical machines, which includes certain simplifications to obtain a tractable model. Indeed, from a machine-engineering viewpoint, the nonlinear magnetic characteristic of the iron core should be considered; due to saturation of the latter the flux is a nonlinear function of the currents.[1] A direct consequence of magnetic saturation is that inductances depend on currents (besides rotor angular positions). Even though saturation plays an essential role for the operation of certain machines such as the surface-mounted PMSM cf., [18], [19], we follow the trend of a unified electrical machine theory in which saturation of the iron core and the effects of the iron yokes are neglected. Therefore, it is assumed that inductances are current independent cf., [17].

We have found in the literature, a few exceptions to this "rule," in the series of fairly recent papers [18], [20]–[22], where surface-mounted PMSM are analyzed with scrutiny thereby considering the physical nonlinearities due to magnetic saturation, however, in a context fundamentally different to this paper's: rotor estimation position for direct-torque control (DTC). See also [23] where an α-β model incorporating saliencies (more precisely, considering inductances as functions of rotor positions only) is used in angular position estimation. In [24], the authors propose a model incorporating effects such as saturation of the iron core, cross-coupling, cross-saturation, and slotting, which yield current and position-dependent flux linkage equations. Flux variations are showed in experimentation. Motivated by the problem of rotor position estimation via saliency "tracking" [25] presents and validates experimentally a model that includes rotor-angles-dependent (but current-independent) inductances. We also mention [26], where the α-β model is used to estimate flux linkage ripple; again, the inductances are considered to depend on rotor positions but not currents.

Variations of the d–q model (1) also have been used in different contexts and with different motivations. Simplified d–q models are often used for instance, neglecting viscous friction—cf., [14], [10] or by considering the stator inductances L_q, L_d to be equal, that is the case of the smooth-air-gap PM machines—cf. [15], [6], [13], [3], [5], [9]. Our main results cover but are not limited to these cases. Other d–q models, such as that in [27] incorporate rotor-position back electromotive force terms in the context of torque ripple minimization; see also [28], where the same model is used in the context of observer design for sensor-less control.

In this paper, we deal with the problem of (angular) velocity control based on the d–q coordinates model (1) thus, we consider the inductances constant but not necessarily equal. To some extent, modelling errors entailed by neglecting saturation may be by considered as parameter uncertainty variations cf., [17] and additive disturbances. Therefore, we show *analytically* that the controlled system under our approach is robust with respect to external perturbations and, in simulations, we show that the controller is also robust with respect to time-varying parameter uncertainties and measurement noise. Other papers where parameter uncertainty, albeit *constant*, is considered include [8], [29], [30], [4]. The last three deal with adaptive control problems in particular, in [4] parameter convergence is showed under the assumption of smooth air-gap (constant equal inductances). In [8], a robustness approach is taken to show, in simulations, that the controlled machine remains practically asymptotically stable. In all of the latter the model (1) is used, except for [30] where it is further assumed that inductances are equal and constant (i.e., $\varepsilon = 0$).

B. Control Model and Control Problem

For control purposes, we recall a standard transformation of system (1) to put the dynamical model in an equivalent form more "comfortable" for control-design purposes; this is used in most of the cited references where the d–q model appears. Let

$$T := \begin{bmatrix} bk & 0 & 0 \\ 0 & k & 0 \\ 0 & 0 & R/L_q \end{bmatrix}; \quad b := \frac{L_q}{L_d}; \quad k := \frac{\beta R}{L_q n_p \psi_r}$$

$$\gamma := -\frac{\psi_r}{kL_q}; \quad \sigma := \frac{\beta L_q}{RJ}; \quad \varepsilon := \frac{n_p b L_q^2 k^2 (L_d - L_q)}{JR^2}$$

$$\tilde{u}_d := \frac{v_d}{Rk}; \quad \tilde{u}_q := \frac{v_q}{Rk}; \quad \tilde{\tau}_L := \frac{L_q^2 \tau_L}{JR^2}.$$

Then, the system (1) may be written in the dimensionless form

$$\frac{d\tilde{\imath}_d}{dt} = -\tilde{\imath}_d + \tilde{\omega}\tilde{\imath}_q + \tilde{u}_d \tag{2a}$$

$$\frac{d\tilde{\imath}_q}{dt} = -\tilde{\imath}_q - \tilde{\omega}\tilde{\imath}_d + \gamma\tilde{\omega} + \tilde{u}_q \tag{2b}$$

$$\frac{d\tilde{\omega}}{dt} = \sigma(\tilde{\imath}_q - \tilde{\omega}) + \varepsilon\tilde{\imath}_d\tilde{\imath}_q - \tilde{\tau}_L \tag{2c}$$

where time has been redefined to $t := Rt'/L_q$ and the state variables as $\tilde{(\cdot)} := T^{-1}(\cdot)$. For more details on this transformation see, e.g., [11], [17].

[1] Such saturation is often called *physical* nonlinearity, not to confuse with *mathematical* nonlinearity.

Next, let the state be defined by $x := [\tilde{\imath}_d \ \tilde{\imath}_q \ \tilde{\omega}]^\top$. Then, defining $\dot{(\cdot)} = \frac{d(\cdot)}{dt}$ the system can be written as

$$\dot{x}_1 = -x_1 + x_3x_2 + \tilde{u}_d \tag{3a}$$
$$\dot{x}_2 = -x_2 - x_3x_1 + \gamma x_3 + \tilde{u}_q \tag{3b}$$
$$\dot{x}_3 = -\sigma(x_3 - x_2) - \tilde{\tau}_L + \varepsilon x_1x_2. \tag{3c}$$

The control problem now comes to finding inputs u_d and u_q such that the system (3) is stabilized over an operating point (or regime). We shall consider that the main variable to control is the velocity ω which, in the coordinates of (3) corresponds to the variable x_3, up to a transformation gain and time rescale. Hence, the goal is to find a pair of controls and values of the desired (current's) reference x_{2d} such that the control goal is achieved. Besides, we stress that with the motivation of achieving *robustness* with respect to external inputs, the goal is to establish uniform global asymptotic stability of the origin of the closed-loop system as opposed to the weaker property that $x_3(t) \to x_{3d}(t)$ as $t \to \infty$.

III. The (Cascades-Based) Control Approach

The approach consists in exploiting the physical properties of the system, in contrast to constructing a Lyapunov function via systematic methods such as backstepping control that often lead to unnecessarily complex nonlinear controls—cf. [4], difficult to implement due to practical constraints (gain restrictions, etc.). Our starting point is to observe that the currents' (3a) and (3b) are "stable" without controls and under a zero-velocity (i.e., $x_3 \equiv 0$) regime, i.e.,

$$\dot{x}_1 = -x_1 \tag{4a}$$
$$\dot{x}_2 = -x_2. \tag{4b}$$

Using the Lyapunov function $V = x_1^2 + x_2^2$, we see that its derivative along the trajectories of (4) yields $\dot{V} = -2(x_1^2 + x_2^2)$. Global exponential stability follows. Let us now consider the velocity variable x_3 as an "external" *input* to the currents' dynamics. This also makes sense if we consider the $x_1 - x_2$ equations as a *fast* electrical system and the x_3 equation as a *slow* mechanical system. With this interpretation in mind, let the "input gain" γ be equal to zero; the electrical equations, without controls, become

$$\dot{x}_1 = -x_1 + x_3x_2 \tag{5a}$$
$$\dot{x}_2 = -x_2 - x_3x_1. \tag{5b}$$

Using $V = x_1^2 + x_2^2$, we again obtain $\dot{V} = -2(x_1^2 + x_2^2)$ and we may conclude that the origin of system (5) is globally exponentially stable, i.e., defining $x_{12} := [x_1 \ x_2]^\top$, we have

$$\|x_{12}(t)\| \le \|x_{12}(t_\circ)\| \mathrm{e}^{-(t-t_\circ)} \quad \forall x_3 \in \mathbb{R}, \quad t \ge t_0 \ge 0.$$

Considering the coordinate transformation and the time-rescale performed in Section II, we obtain an exponentially decaying bound on the currents. The overshoot (maximal absolute value attained during transient) and the decay rate purely depend on the system physical parameters: a simple computation yields

$$\left\| \begin{bmatrix} \frac{1}{bk} & 0 \\ 0 & \frac{1}{k} \end{bmatrix} \begin{bmatrix} i_d(t') \\ i_q(t') \end{bmatrix} \right\| \le \left\| \begin{bmatrix} \frac{1}{bk} & 0 \\ 0 & \frac{1}{k} \end{bmatrix} \begin{bmatrix} i_d(t'_\circ) \\ i_q(t'_\circ) \end{bmatrix} \right\| \mathrm{e}^{-\frac{R}{L_q}(t'-t'_\circ)}.$$

Hence,

$$\left\| \begin{bmatrix} i_d(t') \\ i_q(t') \end{bmatrix} \right\| \le \frac{\max\{1/bk, \ 1/k\}}{\min\{1/bk, \ 1/k\}} \left\| \begin{bmatrix} i_d(t'_\circ) \\ i_q(t'_\circ) \end{bmatrix} \right\| \mathrm{e}^{-\frac{R}{L_q}(t'-t'_\circ)}.$$

Exponential stability of the zero-input system (4) is crucial since it implies that the uncontrolled subsystem, i.e., (3a)–(3b) with $\tilde{u}_q = \tilde{u}_d = 0$, is *input-to-state stable*—cf., [31] from the input x_3. Indeed, for the equations

$$\dot{x}_1 = -x_1 + x_3x_2 \tag{6a}$$
$$\dot{x}_2 = -x_2 - x_3x_1 + \gamma x_3 \tag{6b}$$

we have the following: let $v(t) := 0.5[x_1(t)^2 + x_2(t)^2]$; observe that $0.25[x_1(t)^2 + x_2(t)^2] \le v(t) \le x_1(t)^2 + x_2(t)^2$ and

$$\begin{aligned} \dot{v}(t) &\le -\|x_{12}(t)\|^2 + \gamma\|x_2(t)\|\|x_3(t)\| \\ &\le -\|x_{12}(t)\|^2 + \gamma\|x_{12}(t)\|\|x_3(t)\|. \end{aligned} \tag{7}$$

For any two positive numbers a and b we have, by the triangle inequality, $\gamma ab \le a^2/4 + \gamma^2 b^2$; hence,

$$\dot{v}(t) \le -v(t) + \gamma^2\|x_3(t)\|^2. \tag{8}$$

Integrating on both sides of the inequality above and using the comparison lemma we see that

$$v(t) \le \mathrm{e}^{-(t-t_\circ)}v(t_\circ) + \gamma^2 \int_{t_\circ}^{t} \mathrm{e}^{-(t-\tau)}\|x_3(\tau)\|^2 d\tau. \tag{9}$$

From (9), we see two interesting features that are at the basis of input-to-state stability and of the control strategy followed in this paper: 1) if the "input" $x_3(t)$ is bounded then so is $v(t)$ and hence the currents' magnitudes $\|x_{12}(t)\|$; 2) if, moreover, $x_3(t)$ decays to zero "fast" so do the currents since the convolution integral in (9) decays to zero.

The previous reasoning sets the following criterion for the control design of $\tilde{u}_q$ and $\tilde{u}_d$: it is necessary to define these inputs in a way that the internal stability properties of (3a), (3b) are exploited and "translated" from the zero-current equilibrium to a desired set point. It is also required to design the control in a way that the "input" x_3 in (6) be instead a tracking error that converges to zero. To that end, we analyze now the mechanical (3c).

Now, let us consider $x_1(t)$ and $x_2(t)$ as external "inputs." Under zero load, (3c) reads $\dot{x}_3 = -\sigma x_3$; hence, the origin is exponentially stable for any positive σ. Next, let

$$z(t) := \sigma x_2(t) - \tilde{\tau}_L + \varepsilon x_1(t)x_2(t) \tag{10}$$

then, proceeding as for the states x_1 and x_2 we define $v'(t) := 0.5x_3(t)^2$ and evaluate its derivative along the trajectories of (3c) that is the equation $\dot{x}_3(t) = -\sigma x_3(t) + z(t)$, to obtain $\dot{v}'(t) \le -v'(t) + (1/2\sigma)z(t)^2$; hence,

$$x_3(t)^2 \le \mathrm{e}^{-(t-t_\circ)}x_3(t_\circ)^2 + \frac{2}{\sigma}\int_{t_\circ}^{t} \mathrm{e}^{-(t-\tau)}\|z(\tau)\|^2 d\tau.$$

As before, if $z(t)$ tends to zero so does $x_3(t)$; this holds, i.e., if $\tilde{\tau}_L = 0$ and $x_1(t), x_2(t)$ tend to zero asymptotically—cf., (10). The first requirement holds if we consider zero load, as, i.e., in [4]; the second requirement holds for free for smooth-air-gap

machines ($\varepsilon = 0$), studied, i.e., in [15], [6], [13], [3], [5], and [9].

The fact that $z(t)$ depends on the trajectories $x_1(t)$ and $x_2(t)$ that, in their turn are "driven" by the "input" $x_3(t)$ makes it difficult to conclude that, in general, all signals converge to zero. An obvious counterexample to such supposition is that for certain values of the physical parameters, the system without controls exhibits chaotic behavior—cf., [12], [15], [6]. Yet, it is intuitively clear that the term $-\sigma x_3$ in (3c) and the terms $-x_1, -x_2$ inducing stability in (6a) and (6b), respectively, keep solutions from growing unboundedly.

Summarizing, we view the system (3) as a cascaded system, where $x_3(t)$ is regarded as an *external* input to (3a), (3b) and in turn, $x_1(t)$ and $x_2(t)$ "perturb" the mechanical (3c). That is, the system is in feedback form and not in strict *cascaded* form as, it would be if $x_3(t)$ did not enter as a perturbation into the electrical system Σ_2: (3a)–(3b). While this is obviously a feature of the physical structure of the system and may not be avoided; alternatively, *in* the stability *analysis* we may "forget" about the feedback link if the system Σ_2 is exponentially stable, *independently* of $x_3(t)$.

This is the central idea of cascades-based control design; the formal arguments that support the previous discussions are presented in Appendix A. See also [32].

IV. Set-Point Control

Let us consider the control model of the PMSM, i.e., (3). According to the material presented in the Appendix, in order to formally analyze the system as a cascade, we must make sure that the stability attained for the electrical system Σ_2 is *independent* of the behavior of $x_3(t)$; in particular, we must design the controls so that $x_{12}(t) \to 0$ robustly with respect to the input $x_3(t)$. In this section, we pursue this objective for a desired given *constant* set-point x_{3d}.

A. Known Load

Assume that τ_L is known. The overall constant operating point is set to

$$x_{1d} \neq -\frac{\sigma}{\varepsilon}; \quad x_{2d} := x_{3d} + \vartheta \tag{11}$$

where

$$\vartheta := \frac{\tilde{\tau}_L - \varepsilon x_{1d} x_{3d}}{\varepsilon x_{1d} + \sigma}. \tag{12}$$

The motivation for this choice of set point becomes clear if we reconsider the mechanical equation (3c). We add

$$\pm\varepsilon x_{1d} x_2 \pm \varepsilon x_{1d} x_{2d} \pm \sigma(x_{2d} - x_{3d}) = 0$$

to the right-hand side to obtain, using (11)

$$\dot{x}_3 = -\sigma e_3 + (\sigma + \varepsilon x_{1d}) e_2 + \varepsilon x_2 e_1 \tag{13}$$

where we have defined the error variables $e_i := x_i - x_{id}$ for $i = 1, 2, 3$. The previous equation may be regarded as a dynamic equation of e_3 with "input" $(\sigma + \varepsilon x_{1d}) e_2(t) + \varepsilon x_2(t) e_1(t)$. With the aim at creating a cascaded system, we define the time-invariant *linear* velocity-feedback controller

$$\tilde{u}_d(x_3) := x_{1d} - x_{2d} x_3 \tag{14a}$$

$$\tilde{u}_q(x_3) := x_{2d} + (x_{1d} - \gamma) x_3. \tag{14b}$$

Substituting (14) in the first two equations of (3), we obtain, by direct computation,

$$\dot{x}_1 = -e_1 + x_3 e_2 \tag{15a}$$

$$\dot{x}_2 = -e_2 - x_3 e_1. \tag{15b}$$

Clearly, since x_{1d} and x_{2d} are constant we also have $\dot{e}_i = \dot{x}_i$ for $i = 1, 2, 3$. The resulting error-dynamics equations are

$$\dot{e}_3 = -\sigma e_3 + (\sigma + \varepsilon x_{1d}) e_2 + \varepsilon x_2(t) e_1 \tag{16a}$$

$$\begin{cases} \dot{e}_1 = -e_1 + x_3(t) e_2 \\ \dot{e}_2 = -e_2 - x_3(t) e_1. \end{cases} \tag{16b}$$

which may be regarded as a cascaded system of the form (49). Note that this system is *nonautonomous* even-though, the equivalent *feedback*-interconnected representation

$$\dot{e}_3 = -\sigma e_3 + (\sigma + \varepsilon x_{1d}) e_2 + \varepsilon(e_2 + x_{2d}) e_1 \tag{17a}$$

$$\dot{e}_1 = -e_1 + (e_3 + x_{3d}) e_2 \tag{17b}$$

$$\dot{e}_2 = -e_2 - (e_3 + x_{3d}) e_1 \tag{17c}$$

is time *invariant*. That is, in the system (16), we "see" $x_3(\cdot)$ and $x_2(\cdot)$ as external signals of time in the respective equations where they appear: (16a) forms a *time-varying* subsystem, which depends on the continuous function $t \mapsto x_2$ and has inputs e_1 and e_2; the latter are generated by (16b), which form another nonautonomous subsystem with no inputs.

For the controller (14), (11), we have the following result.

Proposition 1 (Set-Point Control): The system (3) in closed loop with the controller (14) has a globally *exponentially* stable equilibrium point at (11) provided that $\sigma > 0$. □

The following observations are in order:

First, note that other interesting cases considered in the literature are contained in the proposition above. For instance, if the direct-axis and quadrature-axis stator inductances are equal, i.e., if we assume that $\varepsilon = 0$ (commonly assumed in the literature—cf., [15], [6], [13], [3], [5], [9]) the valid operating points include any value for "direct-axis current" x_{1d}.

Second, the result holds based *purely* on the internal stability properties of the system; the only requirement is that $\sigma > 0$. This is a consequence of the cascades-based design and analysis approach that we use; in contrast to this, one may wish to proceed to analyze the stability of the closed-loop system, using Lyapunov's direct method. Let us start with a simple Lyapunov function

$$V(e_1, e_2, e_3) := \frac{1}{2} e_1^2 + e_2^2 + e_3^2. \tag{18}$$

Its total time derivative along the trajectories of the system (17) yields

$$\dot{V} \leq -e_1^2 - e_2^2 - \sigma e_3^2 + (\sigma + \varepsilon x_{1d}) e_2 e_3 + \varepsilon(e_2 + x_{2d}) e_1 e_3.$$

For $\dot{V}$ to be negative definite the *cubic* term $\varepsilon e_2 e_1 e_3$ must be dominated, which is impossible to do, globally, with the quadratic terms $-e_1^2, -e_2^2$, and $-\sigma e_3^2$. Alternatively, one may assume that $\varepsilon = 0$. Yet, even in such case, to dominate the term $\sigma e_2 e_3$ a simple computation yields that $\sigma < 4$ must hold. This

is obviously a stringent condition, e.g., it does not hold in the interesting case when $\sigma = 5.46$, which yields chaotic behavior; we explore this case study in simulations. Note also that La Salle's theorem cannot be used. An alternative is to look for a Lyapunov function yet, the structural problem imposed by the bilinear term e_2e_1 in (17a) makes this task considerably difficult. Finally, following a systematic control design methods such as backstepping—cf., [4], yields in general complex controls, which may depend on the whole state. Other approaches based on the physical structure of the system may lead to simpler controllers. For instance, Hamiltonian-based control is used in [14] and [10] yet, restrictive conditions must be imposed on the controller and, moreover, in the first reference the closed-loop system has more than one equilibrium, which rules out any global result.

B. Unknown Load

Let us assume now that the torque load $\tilde{\tau}_L$ is unknown. In this case, the operating point x_{2d} is unknown and we use the estimate $\hat{\tau}_L$ to define

$$\hat{x}_{2d} := x_{3d} + \frac{\hat{\tau}_L - \varepsilon x_{1d} x_{3d}}{\varepsilon x_{1d} + \sigma} \tag{19a}$$

and we shall design an adaptation law for $\hat{x}_{2d}$. The design strategy, as in [14], relies on our ability to to steer $\hat{x}_{2d}$ to x_{2d} and x_2 to $\hat{x}_{2d}$.

Proposition 2 (Set-Point Control): Consider the system (3) in closed loop with the controller

$$\hat{u}_d := x_{1d} - \hat{x}_{2d} x_3(t) \tag{20a}$$
$$\hat{u}_q := -\gamma x_3(t) + x_{1d} x_3(t) + \hat{x}_{2d} \tag{20b}$$
$$\dot{\hat{\tau}}_L := -\alpha e_3(\varepsilon x_{1d} + \sigma), \qquad \alpha > 0 \tag{20c}$$

with $x_{1d} \neq -\sigma/\varepsilon, \hat{x}_{2d}$ as in (19a). Define $\bar{x}_{2d} := \hat{x}_{2d} - x_{2d}$. Then, the origin of the closed-loop system, i.e., the point $(e_1, e_2, e_3, \bar{x}_{2d}) = (0, 0, 0, 0)$ is globally asymptotically stable provided that $\sigma > 0$. □

Proposition 2, which holds under the same little restrictive assumptions of Proposition 1, establishes global asymptotic stability of the closed-loop system; in *particular*, the load torque $\tilde{\tau}_L$ may be estimated asymptotically. To see this more clearly note, from (11), (12), and (19a) that

$$\bar{\tau} := \hat{\tau}_L - \tilde{\tau}_L = (\varepsilon x_{1d} + \sigma)\bar{x}_{2d}. \tag{21}$$

Proposition 2 follows as a corollary of a more general result, for the case when x_{3d} is a time-varying reference trajectory, i.e., tracking control, solved in the following section.

V. Tracking Control

A. Known Load

The discussion on the cascaded nature of system (16), which is equivalent to system (17), does not rely on considerations such as invariance of the set point (11); hence, as we shall see, it is also useful for the case of tracking control since we regard a time-invariant feedback system as a time-varying cascaded system. This continues to be the rationale behind the proof of the following proposition, which covers the result in Proposition 1.

Proposition 3 (Tracking Control): Let $t \mapsto x_{id}$ be continuously differentiable functions, bounded and with bounded derivatives, such that

$$x_{1d}(t) \neq -\sigma/\varepsilon; \qquad x_{2d} := x_{3d} + \vartheta + \frac{\dot{x}_{3d}}{\varepsilon x_{1d} + \sigma}. \tag{22}$$

Consider the system (3) in closed loop with

$$\tilde{u}_d := x_{1d} - x_{2d} x_3 + \dot{x}_{1d} \tag{23a}$$
$$\tilde{u}_q := x_{2d} + (x_{1d} - \gamma) x_3 + \dot{x}_{2d}. \tag{23b}$$

Then, the closed-loop system has a uniformly globally asymptotically stable equilibrium at the origin. □

Proof: The closed-loop system. First, we derive the error dynamics. Note that (15) and (13) are still valid; then, subtracting $\dot{x}_{1d}$ to both sides of (15a) and $\dot{x}_{2d}$ to both sides of (15b) we obtain the first two closed-loop equations with controls (23), i.e., (17b) and (17c). To analyze the stability of the origin, i.e., of the point $(e_1, e_2, e_3) = (0, 0, 0)$, we write the closed-loop system in terms of the state variables $\xi_1 := e_3$ and $\xi_2 := [e_1 e_2]^\top$ and in the cascaded form:

$$\dot{\xi}_1 := -\sigma\xi_1 + [\varepsilon(\xi_{22} + x_{2d}(t)) \quad \sigma + \varepsilon x_{1d}(t)]\xi_2 \tag{24a}$$
$$\begin{bmatrix} \dot{\xi}_{21} \\ \dot{\xi}_{22} \end{bmatrix} = \begin{bmatrix} -1 & \xi_1(t) + x_{3d}(t) \\ -(\xi_1(t) + x_{3d}(t)) & -1 \end{bmatrix} \begin{bmatrix} \xi_{21} \\ \xi_{22} \end{bmatrix} \tag{24b}$$

or in compact form

$$\dot{\xi}_1 = f_1(\xi_1) + g(t, \xi_2)\xi_2 \tag{25a}$$
$$\dot{\xi}_2 = f_2(t, \xi_2) \tag{25b}$$

where

$$f_1 := -\sigma\xi_1; \quad g(t, \xi_2) := [\varepsilon(\xi_{22} + x_{2d}(t)); \quad \sigma + \varepsilon x_{1d}(t)]$$
$$f_2(t, \xi_2) := \begin{bmatrix} -1 & \xi_1(t) + x_{3d}(t) \\ -\xi_1(t) - x_{3d}(t) & -1 \end{bmatrix} \begin{bmatrix} \xi_{21} \\ \xi_{22} \end{bmatrix}.$$

Stability. For clarity of exposition, at this stage, we assume the following.

Claim 1: Under the conditions of Proposition 3, all trajectories are defined on $[t_\circ, \infty)$ for any $t_\circ \in \mathbb{R} \geq 0$, i.e., the closed-loop system (25) is forward complete.

The proof of this claim is provided in Appendix B. Indeed, if no trajectory explodes in finite time, the following hold:

1) the system $\dot{\xi}_1 = f_1(\xi_1)$ is globally exponentially stable at the origin for any positive value of σ;
2) the system $\dot{\xi}_2 = f_1(t, \xi_2)$ is uniformly globally exponentially stable at the origin: notice that it is of the form of system (5).

To be more precise regarding the second point, let $V(t, \xi_2) := 0.5\|\xi_2\|^2$, its time derivative along the trajectories of (25b) yields $\dot{V} = -2V$; hence,

$$\|\xi_2(t)\| \leq \|\xi_2(t_\circ)\| \mathrm{e}^{-(t - t_\circ)} \qquad \forall t \geq t_\circ. \tag{26}$$

In view of Claim 1, the function $\xi_1(t)$ in (25a) exists for all t and $t_\circ$ and the solutions of (25a) are well defined on compact intervals of time. Therefore, the bound holds for all $t \geq t_\circ$ and all $t_\circ \geq 0$.

Uniform global asymptotic stability of the closed-loop system follows using standard arguments—, e.g., invoking

that the system $\dot{\xi}_1 = f_1(\xi_1) + g(t,\xi_2)\xi_2$ is an exponentially stable *linear* system with a vanishing *integrable* input —cf., [33] and [34, sec. 5.1], Section 5.1; modulo the time-varying nature of the system one may invoke standard results on input-to-state stable systems with vanishing inputs. For results on time-varying cascades, see [35] and Appendix A. To apply Theorem 1, we observe the following.

- Assumption 1 holds with $V = 0.5\xi_1^2$.
- Assumption 2 holds with $\theta_2 \equiv 0$

$$b_M \geq \max_{t\geq 0}\{\|x_{1d}(t)\|, \|x_{2d}(t)\|\}$$
$$\theta_1(\|\xi_2\|) := [\varepsilon\|\xi_2\| + 2b_M + \sigma]\|\xi_2\|.$$

- Assumption 3 holds with $\varphi(s) = s$, in view of (26).

B. Unknown Load

In this case, we define the estimate of the operating point for the normalized q-current variable as

$$\hat{x}_{2d} := x_{3d} + \hat{\vartheta} + \frac{\dot{x}_{3d}}{\varepsilon x_{1d} + \sigma}, \qquad \hat{\vartheta} := \frac{\hat{\tau}_L - \varepsilon x_{1d} x_{3d}}{\varepsilon x_{1d} + \sigma}. \quad (27)$$

Proposition 4 (Tracking Control): Let $t \mapsto x_{id}$ be continuously differentiable functions, bounded and with bounded derivatives satisfying (22). Consider the system (3) in closed loop with

$$\hat{u}_d := x_{1d} - \hat{x}_{2d}x_3(t) + \dot{x}_{1d} \quad (28a)$$
$$\hat{u}_q := -\gamma x_3(t) + x_{1d}x_3(t) + \hat{x}_{2d} + \dot{\hat{x}}_{2d} \quad (28b)$$
$$\dot{\hat{\tau}}_L := -\alpha e_3(\varepsilon x_{1d}(t) + \sigma), \qquad \alpha > 0 \quad (28c)$$

with either $\dot{x}_{1d} \equiv 0$ and $x_{1d} > -\sigma/\varepsilon$ or $\varepsilon = 0$ and $\hat{x}_{2d}$ as in (27). Define $\bar{x}_{2d} := \hat{x}_{2d} - x_{2d}$. Then, the origin of the closed-loop system, i.e., the point $(e_1, e_2, e_3, \bar{x}_{2d}) = (0,0,0,0)$ is uniformly globally asymptotically stable. □

Proof of Proposition 4: The closed-loop equations. Define $\hat{e}_2 := x_2 - \hat{x}_{2d}$; hence, we observe the following useful identities: $\hat{e}_2 - e_2 = -\bar{x}_{2d} := x_{2d} - \hat{x}_{2d}$; $e_2 = \hat{e}_2 + \bar{x}_{2d}$ and $x_2 = \hat{e}_2 + \bar{x}_{2d} + x_{2d}$. We start with e_3 equation of the error dynamics, which is obtained by direct computation, using the latter identities in (13), which is equivalent to the system's (3c) that is,

$$\dot{e}_3 = -\sigma e_3 + (\sigma + \varepsilon x_{1d})\bar{x}_{2d} + (\sigma + \varepsilon x_{1d})\hat{e}_2 + \varepsilon x_2(t)e_1. \quad (29)$$

Now we derive a differential equation for $\bar{x}_{2d}$. To that end, we use the expressions in (27) to obtain

$$\dot{\hat{x}}_{2d} = \dot{x}_{3d} + \dot{\hat{\vartheta}} + \frac{d}{dt}\left\{\frac{\dot{x}_{3d}}{\varepsilon x_{1d} + \sigma}\right\} \quad (30)$$

where, using (28c)

$$\dot{\hat{\vartheta}} = -\alpha e_3 - \frac{(\varepsilon \dot{x}_{1d} x_{3d} + \varepsilon x_{1d}\dot{x}_{3d})}{(\varepsilon x_{1d} + \sigma)} - \frac{(\hat{\tau}_L - \varepsilon x_{1d}x_{3d})\varepsilon \dot{x}_{1d}}{(\varepsilon x_{1d} + \sigma)^2}. \quad (31)$$

Similarly, for $\dot{x}_{2d}$, we find the following. Using (12) and (22) we have

$$\dot{x}_{2d} := \dot{x}_{3d} + \dot{\vartheta} + \frac{d}{dt}\left\{\frac{\dot{x}_{3d}}{\varepsilon x_{1d} + \sigma}\right\} \quad (32)$$

where

$$\dot{\vartheta} = -\frac{(\varepsilon \dot{x}_{1d} x_{3d} + \varepsilon x_{1d}\dot{x}_{3d})}{(\varepsilon x_{1d} + \sigma)} - \frac{(\tilde{\tau}_L - \varepsilon x_{1d}x_{3d})\varepsilon \dot{x}_{1d}}{(\varepsilon x_{1d} + \sigma)^2}. \quad (33)$$

When $\varepsilon = 0$, we have $\dot{\vartheta} = 0$; this corresponds to the case of smooth-air-gap PM machines common in the literature. If $\varepsilon \neq 0$ and $\dot{x}_{1d} \equiv 0$ (constant set-point direct axis current) then

$$\dot{\vartheta} = \frac{-\varepsilon x_{1d}\dot{x}_{3d}}{\varepsilon x_{1d} + \sigma}.$$

Subtracting (32) from (30) and using (33) and (31), we obtain

$$\dot{\tilde{x}}_{2d} := \dot{\hat{\vartheta}} - \dot{\vartheta} \quad (34a)$$
$$= -\alpha e_3 - \frac{(\hat{\tau}_L - \tilde{\tau}_L)\varepsilon \dot{x}_{1d}}{(\varepsilon x_{1d} + \sigma)^2}. \quad (34b)$$

By assumption, either $\dot{x}_{1d} \equiv 0$ or $\varepsilon = 0$; hence,

$$\dot{\tilde{x}}_{2d} = -\alpha e_3. \quad (35)$$

Defining $\xi_1 := [e_3 \bar{x}_{2d}]^\top, \xi_2 := [e_1 \hat{e}_2]^\top$. Equations (29) and (35) can be put together in the compact form

$$\dot{\xi}_1 = f_1(t,\xi_1) + G(t,\xi_1,\xi_2)\xi_2 \quad (36)$$

where $G(t,\xi_1,\xi_2) := [g(t,\xi_1,\xi_2)^\top \ [0\ 0]^\top]^\top$

$$f_1(t,\xi_1) := \begin{bmatrix} -\sigma & \sigma + \varepsilon x_{1d} \\ -\alpha & 0 \end{bmatrix}\xi_1 \quad (37)$$
$$g(t,\xi_1,\xi_2) := [\varepsilon(\xi_{22} + \xi_{12} + x_{2d}(t)) \quad (\sigma + \varepsilon x_{1d}(t))]. \quad (38)$$

Next, we derive the dynamics of ξ_2. For this, we substitute $\hat{u}_d$, as defined in (28a), in place of $\tilde{u}_d$ in (3) and correspondingly, we substitute $\tilde{u}_q$ in (3b) by $\hat{u}_q \pm \gamma x_3(t)$ to obtain

$$\dot{e}_1 = -e_1 + x_3(t)\hat{e}_2 \quad (39a)$$
$$\dot{\hat{e}}_2 = -\hat{e}_2 - x_3(t)e_1 \quad (39b)$$

which can be expressed in compact form, exactly as (25b)-(24b)—only, we have redefined the state variable $\xi_2 = [e_1 \hat{e}_2]^\top$. To proceed further we make the following claim whose proof is included in Appendix B.

Claim 2: The system is forward complete.

Under Claim 2, we may show via Lyapunov's direct method that the system $\dot{\xi}_2 = f_2(t,\xi_2)$ has a globally exponentially stable equilibrium at the origin exactly as we did for system (5) and (25b); hence, (26) holds for $\xi_2 = [e_1^\top \ \hat{e}_2^\top]^\top$.

To show the same property for system $\dot{\xi}_1 = f_1(t,\xi_1)$ observe that, by assumption, either $\varepsilon = 0$ or x_{1d} is constant and $x_{1d} > -\sigma/\varepsilon$; hence, the matrix in (37) is constant. It suffices to chose the parameter α so that the eigenvalues of this matrix are negative; i.e., it suffices to place the poles according to a desired *performance* goal. The eigenvalues are the solutions λ_i of the characteristic polynomial

$$\lambda^2 + \lambda\sigma + \alpha(\varepsilon x_{1d} + \sigma) = 0$$

which have negative real parts for any positive values of α and $(\varepsilon x_{1d}+\sigma)$. The latter holds by assumption; moreover, if $\varepsilon=0$ the condition reduces to $\sigma>0$.

The proof ends by applying Theorem 1 in the Appendix. To see that Assumption 1 holds we introduce

$$v_1(\xi_1):=\frac{1}{2}\|\xi_{11}\|^2+\frac{\varepsilon x_{1d}+\sigma}{2\alpha}\|\xi_{12}\|^2 \tag{40}$$

which is positive definite and radially unbounded if α and $(\varepsilon x_{1d}+\sigma)$ are positive. Since V is quadratic it is easy to see that (51) and (52) hold.

Finally, let $b_M\geq \max_{t\geq 0}\{\|x_{1d}(t)\|,\|x_{2d}(t)\|\}$; then, using (38) we see that

$$\|G(t,\xi_1,\xi_2)\xi_2\|\leq[\varepsilon(\|\xi_2\|+\|\xi_1\|+b_M)+(\varepsilon b_M+\sigma)]\|\xi_2\|$$

so (53) holds with $\theta_1(\|\xi_2\|)=[\varepsilon(\|\xi_2\|+2b_M)+\sigma]\|\xi_2\|$ and $\theta_2(\|\xi_2\|)=\varepsilon\|\xi_2\|$.

Assumption 3 holds uniformly in $\xi_1(t)$ since $\xi_2(t)$ satisfies (26). This concludes the proof of stability for the point $(e_3,\bar{x}_{2d},e_1,\hat{e}_2)=(0,0,0,0)$. Finally, we observe that

$$\begin{bmatrix}\bar{x}_{2d}\\ e_2\end{bmatrix}=\begin{bmatrix}1&0\\1&1\end{bmatrix}\begin{bmatrix}\bar{x}_{2d}\\ \hat{e}_2\end{bmatrix}$$

so the result follows. ∎

VI. Robustness Improvement

It may be reasonably argued that the controls $\tilde{u}_q$ and $\tilde{u}_d$ as defined in (14) may lead to relatively poor performance since no freedom is given to improve, i.e., the convergence rate. Furthermore, as we have discussed in Section II-A even though the model (1) covers a number of case studies used in the literature important physical aspects, which entail inductance variations are not reflected in the d–q coordinates model (1). These phenomena affect the machine performance under specific regimes (low speeds) or at start-off, in this section, we study the robustness of the controlled PMSM (1) with respect to additive disturbances. Indeed, these may be seen as produced by parametric variations and neglected dynamics. In addition, in the following section, we illustrate in simulation the robustness of our controllers with respect to measurement noise.

To start with, note that the controllers proposed so far do not contain any control gain to be tuned, but we have purposely limited ourselves to show the inherent stability properties of the PM machine under pure velocity feedback. In order to stress the robustness properties and possible direct improvements of the controllers previously introduced, let us reconsider the inputs to system (3), i.e., let $\tilde{u}_d(x_3)^*$ and $\tilde{u}_q(x_3)^*$ be, respectively, defined by the right-hand sides of (14), and let us redefine

$$\tilde{u}_d(x_3):=\tilde{u}_d(x_3)^*+\nu_1 \tag{41a}$$
$$\tilde{u}_q(x_3):=\tilde{u}_q(x_3)^*+\nu_2 \tag{41b}$$

where ν_1 and ν_2 are considered to be external (additional) inputs; these may contain perturbations to the system, measurement noise, additional control terms, etc. The closed-loop equations with (3a) and (3b) yield

$$\dot{e}_1=-e_1+x_3(t)e_2+\nu_1 \tag{42a}$$
$$\dot{e}_2=-e_2-x_3(t)e_1+\nu_2. \tag{42b}$$

Define $V(\xi_2):=0.5\xi_2^2$ with $\xi_2=\mathrm{col}[e_1e_2]$ and $\nu=\mathrm{col}[\nu_1\nu_2]$. The time derivative of $V(\xi_2)$ along the trajectories of (42) yields

$$\dot{V}(\xi_2)\leq-\|\xi_2\|^2+\xi_2^\top\nu \tag{43}$$

i.e., the system is output strictly passive—cf., [36]–[38] from the input ν to the output ξ_2. In words, it means that the system seen as a black-box, which transforms inputs ν into the currents (errors) ξ_2 *dissipates energy*. From a robust stability viewpoint, we say that the system is input-to-state stable from the input ν with state ξ_2, which is a property of robust stability with respect to input *disturbances* such as measurement noise. To see more clear, we observe that

$$\xi_2^\top\nu\leq\frac{1}{2}\left(\|\xi_2\|^2+\|\nu\|^2\right)=V(\xi_2)+\frac{1}{2}\|\nu\|^2$$

and we regard (43) along the closed-loop trajectories, i.e., for any $\tau\in[t_\circ,t)$ and $t_\circ\geq 0$, we set $\xi_2=\xi_2(\tau)$ and integrate from $t_\circ$ to t on both sides of

$$\dot{V}(\xi_2(\tau))\leq-V(\xi_2(\tau))+\frac{1}{2}\|\nu(\tau)\|^2$$

to obtain

$$V(\xi_2(t))\leq V(\xi_2(t_\circ))\mathrm{e}^{-(t-t_\circ)}+\frac{1}{2}\int_{t_\circ}^{t}\mathrm{e}^{(\tau-t)}\|\nu(\tau)\|^2d\tau. \tag{44}$$

Let $\|\nu\|_{[t_\circ,t)}$ denote the $\sup_{\tau\in[t_\circ,t)}\|\nu(\tau)\|$; using this in the integrand above we see that

$$V(\xi_2(t))\leq V(\xi_2(t_\circ))\mathrm{e}^{-(t-t_\circ)}+\frac{\|\nu\|^2_{[t_\circ,t)}}{2}\int_{t_\circ}^{t}\mathrm{e}^{(\tau-t)}d\tau \tag{45}$$

hence,

$$\|\xi_2(t)\|\leq\|\xi_2(t_\circ)\|\mathrm{e}^{-\frac{1}{2}(t-t_\circ)}+\frac{1}{2}\|\nu\|_{[t_\circ,t)} \tag{46}$$

i.e., the tracking errors ξ_2 converge to a neighborhood of the origin, proportional to the size of the perturbation.

A natural requirement is to reduce the size of this neighborhood that is, to impose an error tolerance despite the perturbations. This is a direct modification that can be carried out to controls (23) provided we are willing to accept current feedback. Indeed, let ν_1 and ν_2 in (41) be defined by

$$\nu_1:=-k_1e_1+d_1(t) \tag{47a}$$
$$\nu_2:=-k_2e_2+d_2(t) \tag{47b}$$

where $k_i\geq 0$ are design parameters and d_i now play the role of disturbances. Restarting the above computations from (43) we obtain, defining $k_m:=\min\{k_1,k_2\}$ and $d=(d_1d_2)^\top$,

$$\dot{V}(\xi_2)\leq-(k_m+1)\|\xi_2\|^2+\xi_2^\top d.$$

Observing that

$$\xi_2^\top d\leq\frac{1}{2}((k_m+1)\|\xi_2\|^2+\frac{1}{k_m+1}\|d\|^2)$$

we obtain

$$\dot{V}(\xi_2(\tau))\leq-(k_m+1)V(\xi_2(\tau))+\frac{1}{2(k_m+1)}\|d(\tau)\|^2$$

hence,

$$\|\xi_2(t)\|\leq\|\xi_2(t_\circ)\|\mathrm{e}^{-\frac{k_m+1}{2}(t-t_\circ)}+\frac{1}{2(k_m+1)}\|d\|_{[t_\circ,t)}. \tag{48}$$

It is clear that for $k_i = k_m = 0$, i.e., if no current feedback is applied, we recover the inherent robustness expressed by (46); however, for positive values of k_m, we see that the currents' errors converge to the interior of a ball that depends on the norms of the disturbances d but which may be diminished at will by enlarging k_m. In this case, the error tolerance is dictated by physical specifications (maximal size of input voltages $\tilde{u}_q$ and $\tilde{u}_d$).

More "sophisticated" controls may be used: the gains k_1, k_2 may be functions of the state as opposed to constants. For instance, we may decide to make k_i depend on the currents values, i.e., $k_i := k_i(e_i)$. Then, the requirement is that the functions k_i be such that:

1) $k_i(e_i) \geq 0 \qquad \forall e_i \in \mathbb{R}$;
2) there must exist class $\mathcal{K}$ function[2] μ such that

$$\text{whenever } \frac{[k_i(e_i)+1]e_i^2}{\|e_i\|} \geq \|d_i\| \text{ with } i \in \{1,2\}$$
$$\text{we have that } \dot{V}(\xi_2) \leq -\mu(\|\xi_2\|).$$

To see how the last condition enters in play, let us reconsider (43) with ν as in (47) and k_i as defined earlier. We see that

$$\dot{V}(\xi_2) \leq -\sum_{i=1}^{2}[e_i^2[1+k_i(e_i)] - e_i d_i].$$

In these cases, it is not straightforward to integrate the "Lyapunov equations" as done before to obtain bounds with exponential decays; however, under the conditions earlier mentioned, we have that the system is input-to-state stable (ISS) with input d and output ξ_2—cf., [31], [37]. Formally speaking, it may be shown that the currents' error trajectories satisfy the robust bound

$$\|\xi_2(t)\| \leq \beta(\|\xi_2(t_\circ)\|, t - t_\circ) + \mu'(\|d\|_{[t_\circ,t)})$$

where β is a class $\mathcal{K}$ function with respect to the first argument, for each fixed t, and it decreases to zero, for each fixed value of the initial errors $\|\xi_2(t_\circ)\|$. Also, μ' is of class $\mathcal{K}$—cf., [31], [37].

Other practically motivated choices for the control gains are possible. For instance, one may use saturation terms such as $-k_i \mathrm{sat}(e_i)$ with $\mathrm{sat}(\cdot)$ being a smooth saturation function, such as $\tanh(\cdot)$. In this case, however, it is obvious that the robustness improvement is limited by the saturation level.

The functions k_i may also be chosen to depend on the *velocity* errors e_3. For instance, it seems reasonable that, since the variable of main interest is e_3, we make the control gains large only for "large" velocity errors; hence, we define $k_i := k_i(\|e_3\|)$ with k_i of class $\mathcal{K}$.

The proofs for all these cases remain *unchanged*. Moreover, it should be clear that the calculations and discussion mentioned earlier hold for all cases previously studied: set point and tracking with known and unknown load.

VII. Simulations

We have used SIMULINK of MATLAB to test in simulations the performance of the controllers proposed in the previous sections. The simulations' benchmark model is taken from the literature and is as follows: we set the system parameters to values, leading to chaotic behavior in open loop, i.e., $\sigma = 5.46, \gamma = 30, \varepsilon = 0 \tilde{\tau}_L = 10$, and initial state values of 0.01. Several sets of simulations are presented covering the cases with and without disturbances and with and without load estimation. These simulation results illustrate the performance and robustness of all controllers previously introduced.

[2]Continuous, positive strictly increasing and "zero at zero."

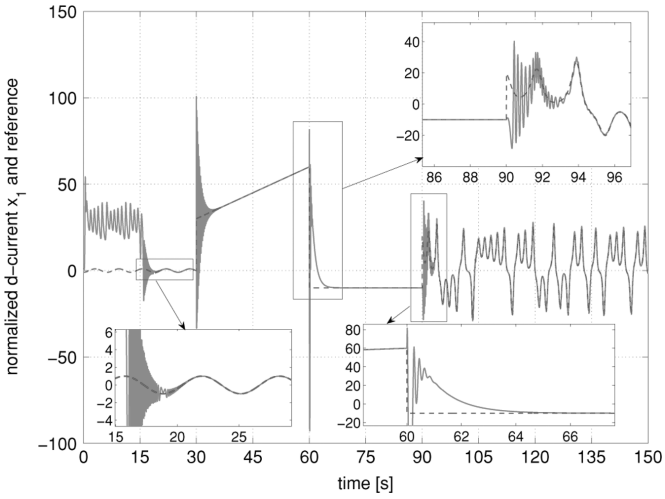

Fig. 1. Graph of the normalized d-current, i.e., x_1 and its reference trajectory. Zooms on reference changes are also shown. Actual response shown in solid line, reference in dashed line.

A. Without Adaptive Control

The simulation experience is as follows: the machine is left to run in open-loop (chaotic) regime for 15 s. At this moment, the controller (23) is "turned on." The results of the simulations are showed in Figs. 1 and 2. The simulation span is of 149 s, and the reference trajectory changes at 30, 60, and 90 s. From 15 to 30 s the reference corresponds to a sinusoid of period 2π followed by a ramp, generated by a step function of amplitude 150 and a "rate delimiter." The reference changes to a step of -10 at 60 s and is left constant up to $t = 90$ s. At this stage, the reference switches to a signal generated by a chaotic Lorenz oscillator. In Fig. 1, we show the reference and actual response for the d-axis normalized current, i.e., the functions $x_1(t)$ and $x_{1d}(t)$. In Fig. 2, we depict the graphs of the system's normalized angular velocity x_3 and its corresponding reference x_{3d}. For better appreciation of transients, we also present zooms on selected windows of the time span. We stress that in the simulations showed in Figs. 1 and 2, we have used the controller (23), i.e., only with velocity measurement and assuming that all parameters are known.

In a second run of simulations, we have introduced up to 20% of time-varying uncertainty in σ and τ_L and additive disturbances generated by a Gaussian random noise signal with zero mean in all three (3). As in all other simulations, control is inactive for $t \in [0, 15)$.

Results are shown in Figs. 3–5. In Fig. 3, we show $x_1(t)$ over $x_{1d}(t)$; in Fig. 4, we show the plots for x_3 and $x_{3d}(t)$; finally, the added noise and perturbations are showed in Fig. 5. In a third run of simulations, we have added the extra current feedback terms in (47) with $k_1 = k_2 = 10$, and the additive perturbation in the velocity equation (3c) has an absolute amplitude of 10, i.e., *20* times as much as in the previous case. The plots for the output of interest, i.e., the (normalized) angular velocity is shown in Fig. 6. Graphs for the normalized d-current

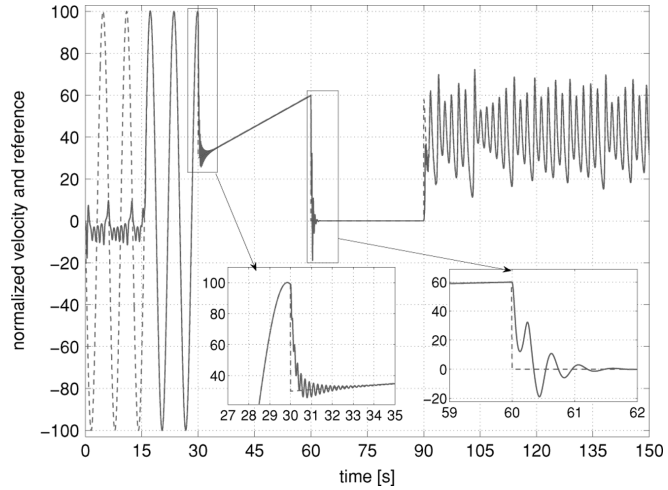

Fig. 2. Graph of the normalized angular velocity, i.e., x_3 and its reference trajectory. Zooms on reference changes are also shown. Actual response shown in solid line, reference in dashed line.

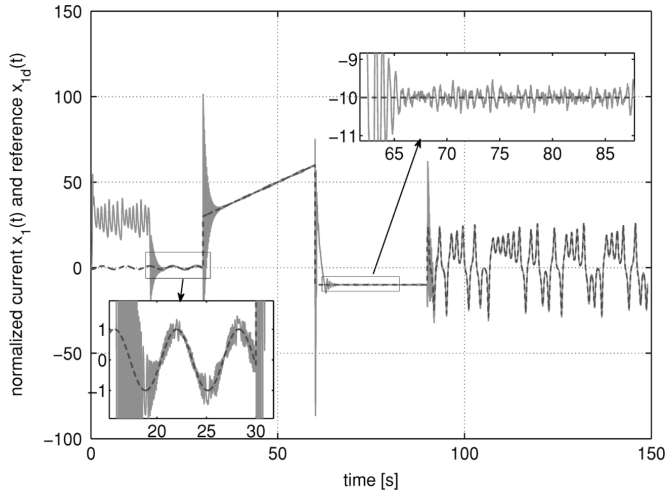

Fig. 3. Graph of the normalized d-current, i.e., x_1 and its reference trajectory. Zooms on reference changes are also shown. Actual response shown in solid line, reference in dashed line.

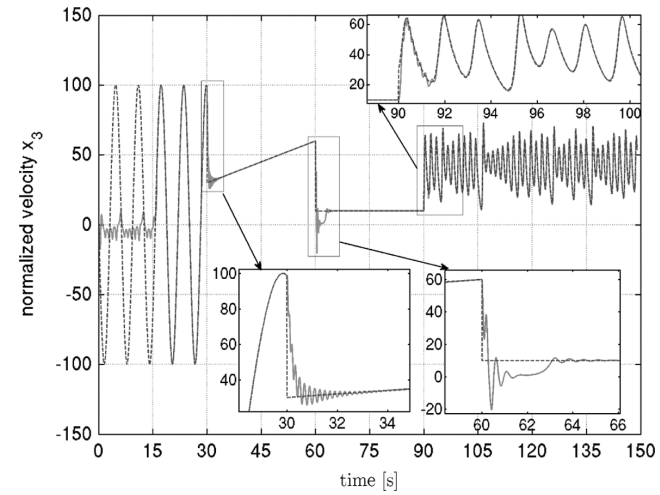

Fig. 4. Simulation under uncertainty and noise. Graph of the normalized angular velocity, i.e., x_3 and its reference trajectory. Zooms on reference changes are also shown. Actual response shown in solid line, reference in dashed line.

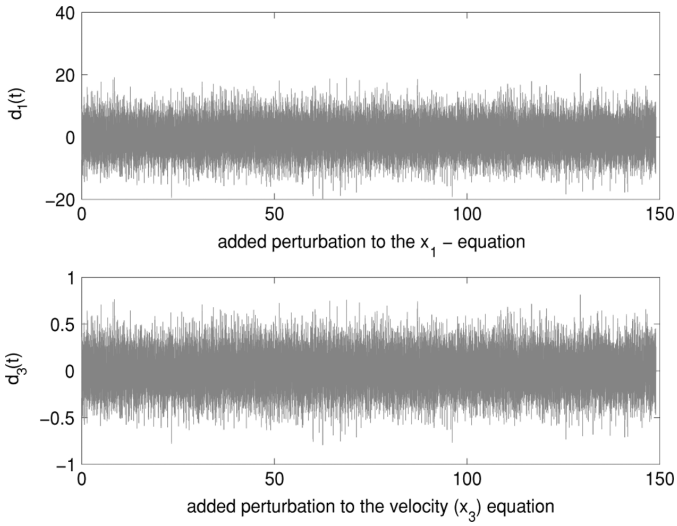

Fig. 5. Simulation under uncertainty and noise. Graphs of additive perturbations $d(t)$cf., (47).

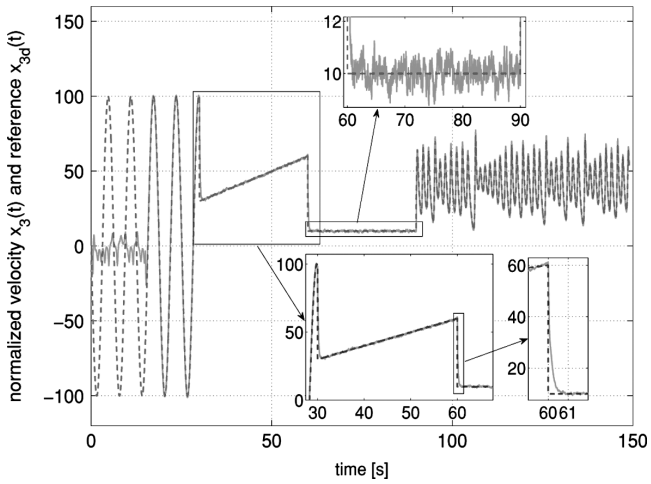

Fig. 6. Simulation under uncertainty and noise. Graph of the normalized angular velocity x_3 and reference trajectory under 20% of parameter uncertainty and additive perturbations $-d_2(t)$ 20 times larger as in Fig. 5. Zooms on transients. Actual response in solid line, reference in dashed line.

are shown in Fig. 7. In particular, one may appreciate the transient improvement due to the additional current feedback and the relatively small steady-state error despite a much larger additive disturbance.

B. With Adaptation

We have run another set of simulations, using the adaptive controller of Proposition 4 under different conditions: with and without current feedback and with and without (time-varying) parametric uncertainty, additive disturbances and measurement noise. When we use the current feedback terms—cf., (47) both gains are set to $k_1 = k_2 = k = 20$. The adaptation gain in (28c) is set to $\alpha = 3$ in all cases. Measurement noise, disturbances, and time-varying parametric uncertainty are generated by random normal Gaussian signals; parametric uncertainty varies from 0 to 20%. The simulation experiment is similar to the previous case: controls are switched on at $t = 15$ s, the normalized reference signal $x_{3d}(t)$ changes from different regimes going from sinusoidal (period $= 2\pi$ and amplitude

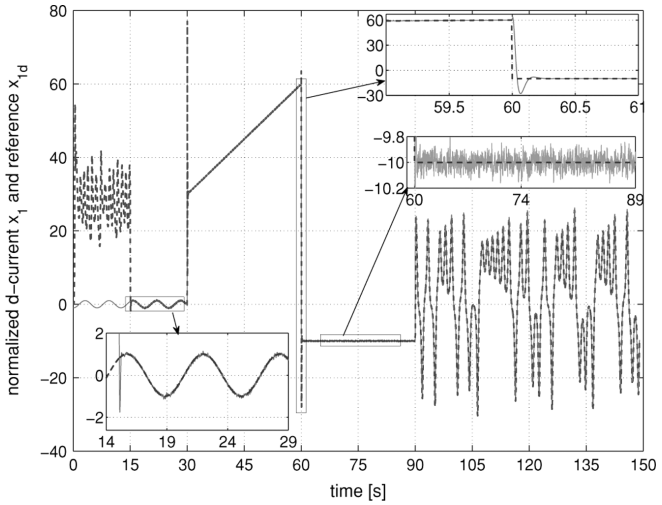

Fig. 7. Simulation under uncertainty and noise. Graph of the d-current x_1 and its reference trajectory under 20% of parameter uncertainty and additive perturbations $-d_2(t)$ 20 times larger as in Fig. 5. Zooms on transients. Actual response in solid line, reference in dashed line.

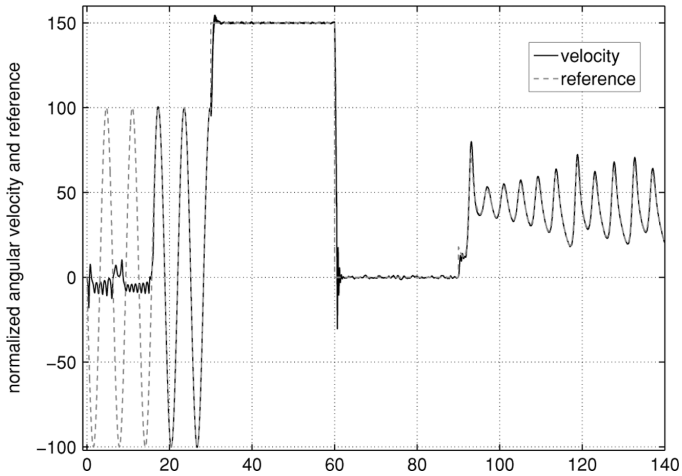

Fig. 8. Graph of the normalized angular velocity and reference in the worst-case scenario: without $k = 0$ in (47), uncertainty and noise.

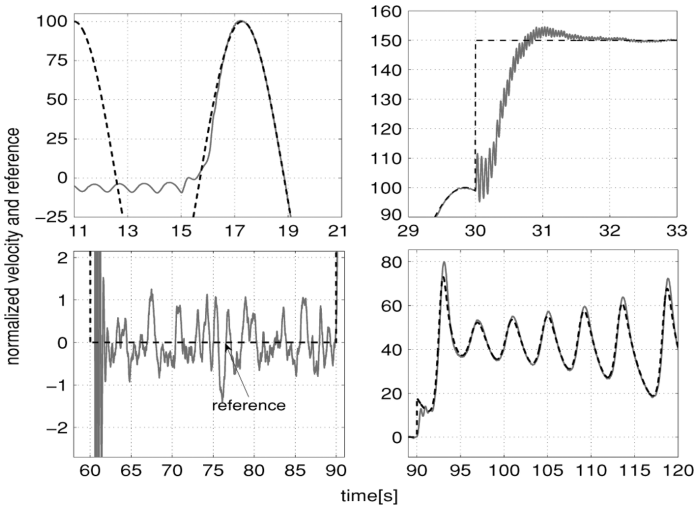

Fig. 9. Graph of the normalized angular velocity and reference in the worst-case scenario: with $k = 0$ in (47), uncertainty and noise. NW plot: transient toward sinusoid of amplitude equal to 100; NE plot: transient from sinusoid toward step of 150; SW plot: transient and tracking of step to zero; SE plot: tracking a Lorenz-generated chaotic reference.

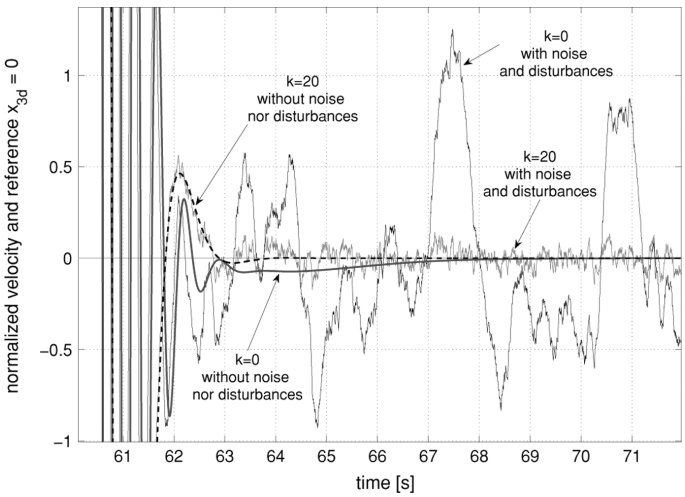

Fig. 10. Zoom on the normalized velocity transient for the second step and reference in four scenarios.

equal to 100) to steps (150 and zero) and finally to a chaotic regime. Reference changes occur at $t = 30$ s, $t = 60$ s, and $t = 90$ s. The simulation results are showed in Figs. 8–15.

In Fig. 8, we show the system's normalized-velocity response in the worst-case scenario: no current feedback—$k = 0$ in (47), presence of additive disturbances, parametric uncertainty and measurement noise. The figure shows both the system's actual trajectory $x_3(t)$ and its reference $x_{3d}(t)$. For better appreciation, zooms on different time windows are depicted in Fig. 9. For the sake of comparison in Fig. 10, we show a zoom on the system's response (normalized velocity $x_3(t)$) in the four different scenarios. The window shows the transient response from the first step (to 150) to a steady-state zero-velocity reference, over the first 10 s. One can appreciate that, in the absence of noise and disturbances, the transient duration is significantly reduced using the state feedback terms in (47). Correspondingly, in the case of parametric uncertainties and noise, the effect of the latter is significantly reduced via the controls from Section VI. In Fig. 11, we show the normalized velocity errors $e_3(t)$ for three different cases with and without noise and disturbances and with $(k = 20)$ and without $(k = 0)$ current feedback. From the zoomed plots, one can clearly appreciate both the transient and steady-state improvement when additional feedback is used, as discussed in Section VI. Also, observe in the lower zoomed window in Fig. 11 the zero-error in the ideal case when there is no parametric uncertainty nor noise even when no extra current feedback is used; that is using the output-feedback adaptive algorithm from Proposition 4. A closer inspection is showed in Fig. 12, where we depict four signals corresponding to the four different scenarios previously described, over a zoomed window around $t = 30$ s. This Figure shows the error transient from a sinusoidal reference to a step of 150. The two plots presenting oscillations correspond to output-feedback control; one may appreciate that the oscillatory behavior is suppressed under current feedback $(k = 20)$. When noise and additive disturbances are present, one may appreciate that the steady-state error is considerably reduced when the additional feedback loops (47) are

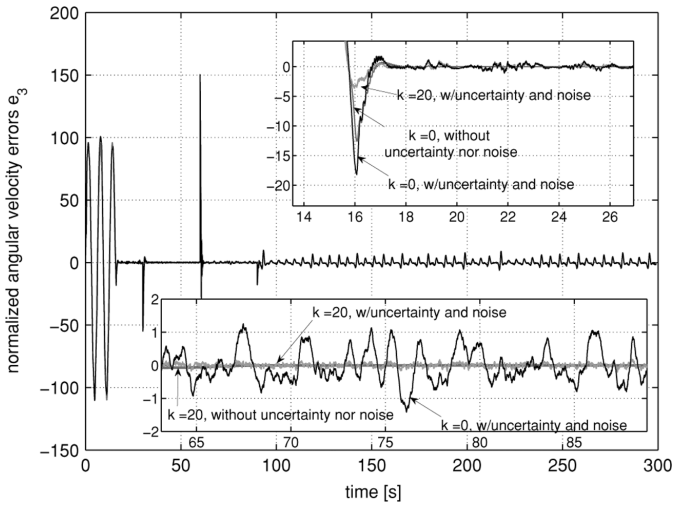

Fig. 11. Graph of the normalized angular velocity errors and zooms. Three cases showed: 1) without extra gain ("$k = 0$") and without uncertainty nor noise; 2) with $k = 0$, uncertainty and noise; and 3) with extra gain $k = 20$ (current feedback), uncertainty and noise.

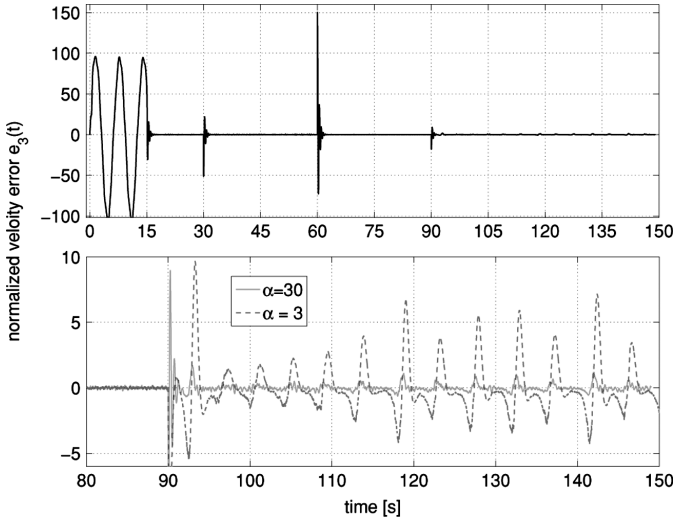

Fig. 13. Zoom on the normalized velocity errors during transient under state-feedback control. Two cases showed: $\alpha = 30$ and $\alpha = 3$; additive disturbances, measurement noise, and time-varying parametric uncertainty present in both cases.

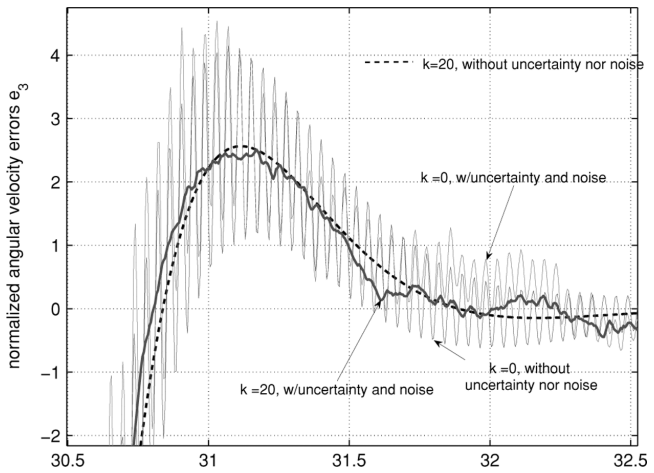

Fig. 12. Zoom on the normalized velocity errors during transient. Four cases showed: 1) without extra gain ("$k = 0$") and without uncertainty nor noise; 2) with $k = 0$, uncertainty and noise; 3) with extra gain $k = 20$ (current feedback) but without uncertainty nor noise; and (4) with uncertainty, noise and current feedback.

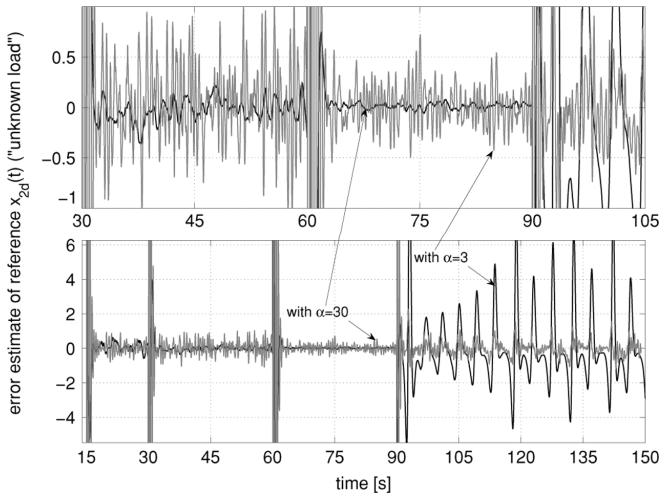

Fig. 14. Zoom on the estimation errors $\hat{e}_2(t)$ during transient and under state-feedback control. Two cases showed: $\alpha = 30$ and $\alpha = 3$; additive disturbances, measurement noise, and time-varying parametric uncertainty present in both cases.

added. The ideal case, i.e., with state feedback, known parameters (except for the load) and absence of disturbances is illustrated by the dashed curve. See also the NE plot on Fig. 9. Finally, we remark from Fig. 11 the steady-state oscillatory behavior of the velocity error when tracking the Lorenz reference (for $t \geq 90$ s); as we show below, this error may be attenuated by increasing the adaptive gain α in (28c).

Similar responses are obtained for the estimated reference $\hat{x}_{2d}$ that depends on the unknown load estimate and for the normalized current $x_1(t)$. The previous observations hold for these curves as well; for comparison, in a third set of simulations, we have kept the current feedback gains as $k_1 = k_2 = k = 20$ and increased the adaptation gain to $\alpha = 30$. The scenario includes additive disturbances, measurement noise, and time-varying parametric uncertainty. The results are showed in Figs. 13–15. In Fig. 13, we show the effect of increasing the adaptive gain, on the velocity error $e_3(t)$ when tracking the Lorenz chaotic reference, to be compared with the error curve in Fig. 11. Similar effects may be appreciated for the estimation error $\hat{e}_2(t)$ depicted over different time windows in Fig. 14. Finally, in Fig. 15, we show the system's responses for the normalized d-current under the same scenarios. Once again, the observations of Section VI as well as the results of Section V are clearly illustrated.

It may be argued that considering random parametric variation is unrealistic. Indeed, as it has been widely validated in experimentation, inductance is, in its most simplistic form, a function of the rotor position. However, the latter depends on the operating regime (constant, chaotic, sinusoidal, etc.) thereby making it hard or impossible to generate a realistic variation for

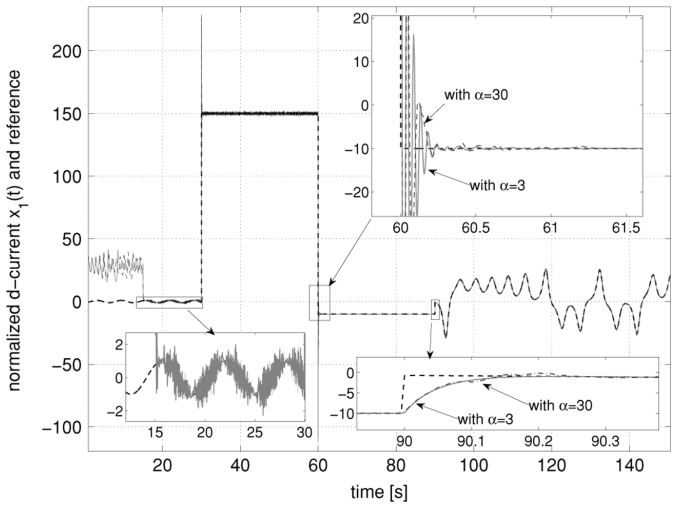

Fig. 15. Normalized d-current $x_1(t)$ and reference under state-feedback control. Two cases showed: $\alpha = 30$ and $\alpha = 3$; additive disturbances, measurement noise, and time-varying parametric uncertainty present in both cases.

L with respect to *time*. Thus, *random* variations within reasonable limits (say $\pm 15\%$) may be considered as "worst-case" scenarios, which cover a variety of possibly more realistic situations[3]. Besides, the study of chaotic systems under the influence of noise has interest of its own, e.g., in the context of synchronization—cf., [39], [40].

VIII. Conclusion

We have showed that both set-point and tracking output regulation of permanent-magnet synchronous ma0chines are achievable via a simple linear output feedback controller, provided that one chooses adequately the operating point for the quadrature axis current. The control is shown to induce global exponential stability in both set-point and tracking control tasks, even in the case of unknown load torque. Stability of control systems under "obvious" modifications to the control algorithms, in view of improving performance and robustness, follow as corollaries from our stability proofs. Future work that comes naturally is experimental validation.

Appendix A
On Cascaded Systems

Consider the cascaded system

$$\dot{\xi}_1 = f_1(t,\xi_1) + g(t,\xi_1,\xi_2) \tag{49a}$$
$$\dot{\xi}_2 = f_2(t,\xi_2) \tag{49b}$$

where, for simplicity, we assume that all the functions are smooth. For the case when f_1, f_2, and g are independent of time, i.e., if the system is autonomous, we know the following fact from [41] and [42]: The origin $\xi \equiv 0$ is uniformly globally asymptotically stable (UGAS) if 1) $\dot{\xi}_1 = f_1(t,\xi_1)$ and $\dot{\xi}_2 = f_2(t,\xi)$ are UGAS and 2) the solutions of (49) are uniformly globally bounded cf., ([43, Lemma. 2]). In general, boundedness of solutions does not come for free and largely relies on the interconnection term g. Indeed, even if it is guaranteed that $x_2(t) \to 0$ asymptotically, large transient overshoots may entail finite-time explosions, i.e., $\|x_1(t)\| \to \infty$ as $t \to t_e < \infty$. If otherwise, that is if the trajectories are defined for all t we say that the system is *forward complete*. This property cannot be overestimated; it goes beyond *academic* examples. For instance, for the system $\dot{x} = \pm x^2$ it can be shown by solving the differential equation, that there is finite-escape time for specific initial conditions; this is due to the square exponent in the term x^2. For the sake of comparison, let us recall that, for Lagrangian systems, the Coriolis and centrifugal forces matrix is of order square with respect to generalized velocities cf.,[44].

The following example, which is somewhat reminiscent of the situation we encounter in cascaded-based control of the PM machine, aims at illustrating such stumbling blocks.

Consider the system

$$\Sigma_1 : \dot{\xi}_1 = -\xi_1^3 + \xi_1^3\xi_2 \tag{50a}$$
$$\Sigma_2 : \dot{\xi}_2 = -(1+\xi_1^2)\xi_2. \tag{50b}$$

We observe the following: 1) defining $V_1 = \xi_1^2$ we have $\dot{V} = -2\xi_1^4 < 0$; hence $\dot{\xi}_1 = -\xi_1^3$ is asymptotically stable and 2) defining $V_2 = \xi_2^2$ we get $\dot{V}_2 \le -2\xi_2^2 - 2\xi_1^2\xi_2^2 \le -\xi_2^2$. That is, $\dot{V}_2$ is negative definite, independently of ξ_1^2. We would like to regard the subsystem Σ_2 along the trajectories $\xi_1(t)$ thereby "forgetting" the feedback loop established by ξ_1 in (50b). While this seems possible under the previous (standard) Lyapunov arguments, strictly speaking, the system

$$\Sigma_2' : \dot{\xi}_2 = -(1+\xi_1(t)^2)\xi_2$$

is ill-defined if $\xi_1(t)$ explodes in finite time. That is, all what we may conclude from the previous Lyapunov analysis is roughly that, "while the trajectories do not explode, $\xi_2(t)$ decreases exponentially fast," which implies that "if (and only if) the trajectories $\xi_1(t)$ do not explode the system Σ_2 is exponentially stable." For a recent formal treatment of feedback systems viewed as cascades see [32].

When taking care of the technical issues discussed earlier, feedback systems may be regarded as cascaded systems. Then, one can use (among others) the following result on stability of cascaded systems (49).

Theorem 1: Let the origin of systems $\xi_1 = f_1(t,\xi_1)$ and $\xi_2 = f_2(t,\xi_2)$ be UGAS and Assumptions 1–3 below hold. Then, the origin of (49) is UGAS.

Assumption 1: There exist constants $c_1, c_2, \eta > 0$ and a Lyapunov function $V(t,\xi_1)$ for $\xi_1 = f_1(t,\xi_1)$ such that $V : \mathbb{R}_{\ge 0} \times \mathbb{R}^n \to \mathbb{R}_{\ge 0}$ is positive definite, radially unbounded, $\dot{V}(t,\xi_1) \le 0$ and

$$\left\|\frac{\partial V}{\partial \xi_1}\right\| \|\xi_1\| \le c_1 V(t,\xi_1) \quad \forall \|\xi_1\| \ge \eta \tag{51}$$
$$\left\|\frac{\partial V}{\partial \xi_1}\right\| \le c_2 \quad \forall \|\xi_1\| \le \eta. \tag{52}$$

Assumption 2: There exist two continuous functions $\theta_1, \theta_2 : \mathbb{R}_{\ge 0} \to \mathbb{R}_{\ge 0}$, such that $g(t,\xi_1,\xi_2)$ satisfies

$$\|g(t,\xi_1,\xi_2)\| \le \theta_1(\|\xi_2\|) + \theta_2(\|\xi_2\|)\|\xi_1\|. \tag{53}$$

[3]In simulations not showed here for space constraints, we use lookup tables based on experimental data taken from ([18, Fig. 4],); the results are *better*.

Assumption 3: There exists a class $\mathcal{K}$ function $\varphi(\cdot)$ such that, for all $t_\circ \geq 0$, the trajectories of the system (49b) satisfy

$$\int_{t_\circ}^{\infty} ||\xi_2(t; t_\circ, \xi_2(t_\circ))||dt \leq \varphi(||\xi_2(t_\circ)||). \tag{54}$$

APPENDIX B

A. Proof of Claim 1

Consider system (25). Let

$$V = \frac{1}{2}\left(\xi_1^2 + ||\xi_2||^2\right).$$

The time derivative of V along the closed-loop trajectories of (25) yields

$$\dot{V} \leq -\sigma\xi_1^2 - ||\xi_2||^2 + ||\xi_1||\ ||\xi_2||\ ||g(t, \xi_2)||.$$

Let $t_{\max} < \infty$ determine the maximal interval of existence of the closed-loop solutions, i.e., let $\xi(\cdot)$ be an absolutely continuous function defined on $[t_\circ, t_{\max})$ and let $||\xi(t_{\max})|| \to \infty$ as $t \to t_{\max}$. Define $v(t) := V(t, \xi(t))$ then, on the interval of existence we have

$$\begin{aligned}\dot{v}(t) &\leq ||\xi_1(t)||\ ||\xi_2(t)||\ ||g(t, \xi_2(t))|| \\ &\leq ||\xi_1(t)||^2 + ||\xi_2(t)||^2[c_1 + c_2||\xi_2(t)||]^2\end{aligned}$$

however, on the same interval $[t_\circ, t_{\max})$, we have $||\xi_2(t)|| \leq ||\xi_2(t_\circ)||$. Define $c_3(||\xi_2(t_\circ)||) := [c_1 + c_2||\xi_2(t_\circ)||]^2$ and $c_4(||\xi_2(t_\circ)||) := 2\max\{1, c_3(||\xi_2(t_\circ)||)\}$ then,

$$\dot{v}(t) \leq c_4(||\xi_2(t_\circ)||)v(t)\ \forall t \in [t_\circ, t_{\max}).$$

We have, on one hand,

$$\int_{t_\circ}^{t_{\max}} \frac{\dot{v}(t)dt}{c_4 v(t)} \leq t_{\max} - t_\circ$$

and, since

$$\lim_{t \to t_{\max}} v(t) = \infty$$

we have on the other hand[4]

$$\int_{t_\circ}^{t_{\max}} \frac{\dot{v}(t)dt}{c_4 v(t)} = \int_{v(t_\circ)}^{\infty} \frac{dv}{c_4 v} = \ln(c_4 v)\Big|_{v(t_\circ)}^{+\infty} = +\infty.$$

We conclude that $t_{\max}$ cannot be finite.

B. Proof of Claim 2

Consider the system (36), (39). Let $[t_\circ, t_{\max})$ denote the maximal interval of definition of solutions of (39) and define

$$v_2(\xi_2(t)) := \frac{1}{2}||\xi_2(t)||^2.$$

The total time derivative of v_2 yields, using (39),

$$\dot{v}_2(\xi_2(t)) = -||\xi_2(t)||^2.$$

[4]We consider, without loss of generality, that $v(t_\circ) \neq 0$.

That is,

$$||\xi_2(t)|| \leq ||\xi_2(t_\circ)||e^{-(t-t_\circ)} \qquad \forall t \in [t_\circ, t_{\max}). \tag{55}$$

The interconnection term g in (36) satisfies, along solutions, and on the interval of definition of the latter

$$||g(t, \xi_1(t), \xi_2(t))|| \leq c + \varepsilon[||\xi_{12}(t)|| + ||\xi_{22}(t)||]$$

where c is a positive number independent of the initial conditions—it depends only on bounds on the reference trajectories $x_{2d}(t)$ and $x_{3d}(t)$. Using this and (40), it is direct to obtain that the time derivative of

$$v(t) := v_2(\xi_2(t)) + v_1(\xi_1(t)) \tag{56}$$

along the trajectories generated by (36) and (39), satisfies

$$\begin{aligned}&\dot{v}(t) \leq \\ &\quad c'||\xi_1(t)||\ \ ||\xi_2(t)|| + \varepsilon'[||\xi_1(t)||^2||\xi_2(t)|| + ||\xi_2(t)||^2||\xi_1(t)||]\end{aligned}$$

where $(\cdot)' := (\cdot)\max\{1, (\varepsilon x_{1d} + \sigma)/(\alpha)\}$. Using the triangle inequality on the bound aforementioned and (55) we obtain that there exists $c'' : \mathbb{R} \to \mathbb{R}$ such that

$$\dot{v}(t) \leq c''(||\xi_2(t_\circ)||)v(t) \qquad \forall t \in [t_\circ, t_{\max}).$$

Integrating on both sides and proceeding as in the proof of Claim 1, we conclude that $t_{\max} = +\infty$.

ACKNOWLEDGMENT

The author would like to thank A. Sánchez for discussions held on electrical machines' modelling and W. Pasillas for his helpful remarks on numeric simulation.

REFERENCES

[1] K. T. Chau and J. H. Chen, "Modeling, analysis, and experimentation of chaos in a switched reluctance drive system," *IEEE Trans. Circuit Syst. I, Fundam. Theory Appl.*, vol. 50, no. 5, pp. 712–716, May 2003.

[2] J. H. Chen, K. T. Chau, S. M. Siu, and C. C. Chan, "Experimental stabilization of chaos in a voltage-mode DC drive system," *IEEE Trans. Circuit Syst. I, Fundam. Theory Appl.*, vol. 47, no. 7, pp. 1093–1095, Jul. 2000.

[3] Z. Wang and K. T. Chau, "Anti-control of a permanent-magnet DC motor system for vibratory compactors," *Chaos Solitons Fractals*, vol. 36, pp. 694–708, 2008.

[4] D. Q. Wei, X. S. Luo, B. H. Wang, and J. Q. Fang, "Robust adaptive dynamic surface control of chaos in permanent magnet synchronous motor," *Phys. Lett. A*, vol. 363, no. 1–2, p. 71, 2007.

[5] H. P. Ren and C. Z. Han, "Chaotifying control of permanent-magnet synchronous motor," in *Proc. Power Electron. Motion Control Conf.*, 2006, vol. 1, pp. 1–5.

[6] X. Ge and J. Huang, "Chaos control of permanent-magnet synchronous motor," in *Proc. Int. Conf. Electrical Machines and Systems*, 2005, vol. 1, pp. 484–488.

[7] Z. Meng, C. Sun, Y. An, J. Cao, and P. Gao, "Chaos anti-control of permanent-magnet synchronous motor based on model matching," in *Proc. Int. Conf. Electrical Machines and Systems*, Seoul, Korea, 2007, pp. 1748–1752.

[8] H. Ren and D. Liu, "Nonlinear feedback control of chaos in permanent-magnet synchronous motor," *IEEE Trans. Circuit Syst. II, Exp. Briefs*, vol. 53, no. 1, pp. 45–50, Jan. 2006.

[9] D. Liu, H. Ren, and X. Liu, "Chaos control in permanent-magnet synchronous motor," in *Proc. Int. Symp. Circuits Syst.*, 2004, vol. 4, pp. 732–735.

[10] H. Yu, H. Wang, and K. Zhao, "Energy-shaping of PM synchronous motor based on Hamiltonian systems theory," in *Proc. Int. Conf. Electrical Machines and Systems*, 2005, vol. 2, pp. 1549–1553.

[11] N. Hemati, "Strange attractors in brushless DC motors," *IEEE Trans. Circuit Syst. I, Fundam. Theory Appl.*, vol. 41, no. 1, pp. 40–45, Jan. 1994.
[12] Z. Li, J. B. Park, Y. H. Joo, B. Zhang, and G. Chen, "Bifurcations and chaos in a permanent-magnet synchronous motor," *IEEE Trans. Circuit Syst. I, Fundam. Theory Appl.*, vol. 49, no. 3, pp. 383–387, Mar. 2002.
[13] C. Cai, Z. Xu, and W. Xu, "Converting chaos into periodic motion by state-feedback control," *Automatica*, vol. 38, pp. 1927–1933, 2002.
[14] V. Petrović, R. Ortega, and A. M. Stanković, "Interconnection and damping assignement approach of PM synchronous motors," *IEEE Trans. Control Syst. Technol.*, vol. 9, no. 6, pp. 811–820, Nov. 2001.
[15] Z. Li, B. Zhang, and Z. Mao, "Analysis of the chaotic phenomena in permanent-magnet synchronous motors based on Poincaré map," in *Proc. 3rd World Congr. Intell. Control Autom.*, Hefei, China, 2000, pp. 3255–3260.
[16] N. Hemati and H. Kwati, "Bifurcation of equilibria and chaos in permanent-magnet machines," in *Proc. 32nd. IEEE Conf. Decision Contr.*, San Antonio, TX, USA, 1993, pp. 475–480.
[17] C. J. Retter, *Matrix and Space-Phasor Theory of Electrical Machines*. Budapest: Akadémiai Kiadó, 1987.
[18] Y. Yan, J. Zhu, H. Lu, Y. Guo, and S. Wang, "A PMSM model incorporating structural and saturation saliencies," in *Proc. 8th Int. Conf. Electrical Machines and Systems*, Sept. 27–29, 2005, vol. 1, pp. 194–199.
[19] D. S. Maric, S. Hiti, C. C. Stancu, J. M. Nagashima, and D. B. Rutledge, "An application of a constrained adaptive lattice-structure allpass-based notch filter for advanced control of surface-mounted permanent-magnet synchronous drives," *IEEE Trans. Circuits Syst. I, Fundam. Theory Appl.*, vol. 46, no. 12, pp. 1513–1516, Dec. 1999.
[20] Y. Yan, J. Zhu, Y. Guo, and H. Lu, "Modeling and simulation of direct torque controlled PMSM drive system incorporat structural and saturation saliencies," in *Proc. 41st Ind. Appl. Conf.*, Oct. 27–29, 2006, vol. 1, pp. 76–83.
[21] Y. Yan, J. Zhu, H. Lu, Y. Guo, and S. Wang, "A direct torque controlled surface mounted PMSM drive with initial rotor position estimation based on structural and saturation saliencies," in *Proc. 42nd Ind. Appl. Conf.*, Sept. 23–27, 2007, vol. 1, pp. 683–689.
[22] Y. Ying, Z. Jianguo, G. Youguang, and J. Jianxun, "Numerical simulation of a PMSM model considering saturation saliency for initial rotor position," in *Proc. 27th Chin. Control Conf.*, Kunming, China, July 16–18, 2008, pp. 114–118.
[23] V. Petrović and A. M. Stanković, "Saliency-based position estimation in PM synchronous motors," in *Proc. Ind. Appl. Conf.*, 2001, vol. 2, pp. 801–806.
[24] M. Hadžiselimović, G. Štumberger, B. Štumberger, and I. Zagradišnik, "Magnetically nonlinear dynamic model of synchronous motor with permanent magnets," *J. Magnets Magn. Mater.*, no. 317, pp. 257–260, 2007.
[25] L. Wang and R. D. Lorenz, "Rotor position estimation for permanent magnet synchronous motor using saliency-tracking self-sensing method," in *Proc. Conf. Ind. Appl.*, 2000, vol. 1, pp. 445–450.
[26] X. Xi, Z. Meng, L. Yongdong, and L. Min, "On-line estimation of permanent magnet flux linkage ripple for PMSM based on a Kalman filter," in *Proc. IECON*, 2006, pp. 1171–1175.
[27] V. Petrović, R. Ortega, A. M. Stanković, and G. Tadmor, "Design and implementation of an adaptive controller for torque ripple minimization in PM synchronous motors," *IEEE Trans. Power Electron.*, vol. 15, no. 5, pp. 871–880, Sept. 2000.
[28] F. Poulin, L. Praly, and R. Ortega, "An observer for permanent magnet synchronous motors with application to sensorless control," in *47th. IEEE Conf. Decision Contr.*, Cancún, México, Dec. 9–11, 2008, pp. 5390–5395.
[29] N. Goléa, A. Goléa, and M. Kadjoudj, "Robust MRAC adaptive control of PMSM drive under general parameters uncertainties," in *Proc. IEEE Int. Conf. Ind. Technol.*, 2006, pp. 1533–1537.
[30] J. Kabziński, "Adaptive backstepping control of a completely unknown permanent magnet motor," in *Proc. Eur. Conf. Power Electron. Appl.*, Sept. 2–5, 2007, pp. 1–10.
[31] E. Sontag, "Smooth stabilization implies coprime factorization," *IEEE Trans. Autom . Contr.*, vol. 34, no. 4, pp. 435–443, Apr. 1989.
[32] A. Loría, "From feedback to cascade-interconnected systems: Breaking the loop," in *Proc. 47th. IEEE Conf. Decision Contr.*, Cancun, Mexico, Dec. 9–11, 2008, pp. 4109–4114.
[33] C. Desoer and M. Vidyasagar, *Feedback Systems: Input-Output Properties*. New York: Academic Press, 1975.
[34] H. Khalil, *Nonlinear Systems*, 2nd ed. New York: Macmillan, 1996.
[35] A. Loría and E. Panteley, , F. Lamnabhi-Lagarrigue, A. Loría, and E. Panteley, Eds., "Advanced topics in control systems theory. Lecture Notes in Control and Information Sciences," in *Cascaded Nonlinear Time-Varying Systems: Analysis and Design*. London: Springer-Verlag, 2005.
[36] D. Hill and P. Moylan, "The stability of nonlinear dissipative systems," *IEEE Trans. Autom. Control*, vol. 21, no. 5, pp. 708–711, Oct. 1976.
[37] H. Khalil, *Nonlinear systems*, 3rd ed. New York: Prentice Hall, 2002.
[38] R. Ortega, A. Loría, P. J. Nicklasson, and H. Sira-Ramírez, *Passivity-based Control of Euler-Lagrange systems: Mechanical, electrical and electromechanical applications*, ser. Comunications and Control Engineering. London: Springer-Verlag, 1998, ISBN 1-85233-016-3.
[39] E. Sánchez, M. A. Matías, and V. P.-M. nuzuri, "An experimental setup for studying the effect of noise on Chua's circuit," *IEEE Trans. Circuit Syst. I, Fundam. Theory Appl.*, vol. 46, no. 4, pp. 517–520, Apr. 1999.
[40] Z. Zhu, H. Leung, and Z. Ding, "Optimal synchronization of chaotic systems in noise," *IEEE Trans. Circuit Syst. I, Fundam. Theory Appl.*, vol. 46, no. 11, pp. 1320–1329, Nov. 1999.
[41] P. Seibert and R. Suárez, "Global stabilization of nonlinear cascaded systems," *Syst. Control Lett.*, vol. 14, pp. 347–352, 1990.
[42] E. D. Sontag, "Remarks on stabilization and input-to-state stability," in *Proc. 28th. IEEE Conf. Decision Control*, Tampa, FL, 1989, pp. 1376–1378.
[43] E. Panteley and A. Loría, "Growth rate conditions for stability of cascaded time-varying systems," *Automatica*, vol. 37, no. 3, pp. 453–460, 2001.
[44] H. Goldstein, *Classical Mecanics*. Reading, MA: Adisson-Wesley, 1974.

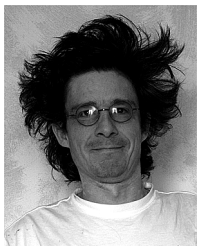

Antonio Loria (S'90–M'91) was born in Mexico City in 1969. He received the B.Sc. degree in electronic engineering from the Monterrey Institute of Technology and Higher Education, Monterrey, Mexico, in 1991, and the M.Sc. and Ph.D. degrees in control engineering from the University of Technology of Compiegne, Compiegne, France, in 1993 and 1996, respectively.

From December 1996 to December 1998, he was successively an Associate Researcher at the University of Twente, The Netherlands; Norwegian University of Science and Technology, Norway, and the Center for Control Engineering and Computation, University of California, Santa Barbara, CA. He has the honor of holding a research position as the Directeur de Recherche (Senior Researcher) at the French National Centre of Scientific Research. Since December 2002, he has been with the Laboratoire de Signaux et Systemes, Supelec, Gif-sur-Yvette, France. His current research interests include control systems theory and practice, electrical systems, and analysis and control of chaos.

Dr. Loria is a member of the IEEE Control Systems Society Conference Editorial Board. He has served as an Associate Editor of the IEEE TRANSACTIONS ON AUTOMATIC CONTROL, and also of *Systems and Control Letters* and *Automatica*.